Article

Synergistic Model of Cardiac Function with a Heart Assist Device

Eun-jin Kim [1,2,*] and **Massimo Capoccia** [3]

[1] Fluid and Complex Systems Research Centre, Coventry University, Coventry CV1 2TT, UK
[2] School of Mathematics and Statistics, University of Sheffield, Sheffield S3 7RH, UK
[3] Aortic and Cardiac Surgery, Royal Brompton Hospital, Sydney Street, Chelsea, London SW3 6NP, UK; capoccia@doctors.org.uk
[*] Correspondence: ejk92122@gmail.com; Tel.: +44-2477-659041

check for updates

Abstract: The breakdown of cardiac self-organization leads to heart diseases and failure, the number one cause of death worldwide. The left ventricular pressure–volume relation plays a key role in the diagnosis and treatment of heart diseases. Lumped-parameter models combined with pressure–volume loop analysis are very effective in simulating clinical scenarios with a view to treatment optimization and outcome prediction. Unfortunately, often invoked in this analysis is the traditional, time-varying elastance concept, in which the ratio of the ventricular pressure to its volume is prescribed by a periodic function of time, instead of being calculated consistently according to the change in feedback mechanisms (e.g., the lack or breakdown of self-organization) in heart diseases. Therefore, the application of the time-varying elastance for the analysis of left ventricular assist device (LVAD)–heart interactions has been questioned. We propose a paradigm shift from the time-varying elastance concept to a synergistic model of cardiac function by integrating the mechanical, electric, and chemical activity on microscale sarcomere and macroscale heart levels and investigating the effect of an axial rotary pump on a failing heart. We show that our synergistic model works better than the time-varying elastance model in reproducing LVAD–heart interactions with sufficient accuracy to describe the left ventricular pressure–volume relation.

Keywords: cardiac function; modeling; self-organization; lumped-parameter model; left ventricular pressure–volume relation; LVAD

1. Introduction

Self-organization is a novel phenomenon in complex systems, whereby a macroscopic order emerges and is maintained in the midst of complexity [1]. One remarkable manifestation of self-organization is homeostasis in biosystems, known to be absolutely critical to the sustainability of living organisms. As one of most beautiful and important examples of self-organized biosystems [2], the human heart is a mechanical pump acting as a main force driving blood throughout the body via the circulatory system, supplying oxygen and nutrients to the tissues, and removing carbon dioxide and other waste products. The action of this mechanical pump is tightly regulated and is self-organized by feedback mechanisms among mechanical, electric, and chemical activities. Furthermore, cardiac function is self-organized and synchronized across scales, from microscale sarcomere to macroscale organ levels. Unfortunately, the breakdown of self-organization leads to heart diseases and failure, the number one cause of death worldwide.

Mechanical circulatory support with rotary blood pumps, such as HeartMate II (an axial pump manufactured by Thoratec Corporation, Pleasanton, CA, USA) [3] and HeartWare ventricular assist device (HVAD: a centrifugal pump manufactured by Medtronic, Minneapolis, MN, USA) [4], is a

recognized treatment for advanced heart failure patients, either as a bridge to transplant or recovery or ultimately as a long-term solution for noneligible candidates (destination therapy). Although very successful, the insertion of a left ventricular assist device (LVAD) remains associated with complications such as pump thrombosis, stroke, bleeding, and right heart failure, which affect outcomes [5–10]. It is, thus, crucial to increase our understanding of feedback mechanisms and heart–LVAD interactions.

The single most powerful measure to understand heart function and differentiate normal from pathological heart, as well as to diagnose or treat different cardiac pathology, is the relation between left ventricular pressure and volume—the so-called P–V loop. In particular, pressure–volume relation applied to lumped-parameter representation of the cardiovascular system has important clinical applications [6,11], owing to great flexibility in simulating the hemodynamics of different cardiovascular conditions and therapeutic interventions at a low computational cost, facilitating a personalized therapy [11]. However, the traditional approach heavily relies on the time-varying elastance model [11–16], where the ratio of the pressure to the volume (minus the ventricular volume at zero pressure) is prescribed as a periodic (double-Hill) function of time for a given heart rate, varying between given E_{max} (the maximum value of E) and minimum E_{min} (the minimum value of E). Although the time-varying elastance model has been useful in understanding the pressure–volume relation in different types of mammals, it is empirically based on (almost) physiological data where the heart is regulated internally. Thus, its validity in extreme, pathological conditions (such as in [17] in a study on mice) is questionable. For instance, when heart rhythm is not regular but chaotic (as in the case of fibrillation), elastance will also be chaotic rather than a simple periodic function. This issue is particularly important for the treatment of a failing heart requiring the insertion of a LVAD. In particular, since the device is connected in parallel between the aorta and the left ventricle to relieve its load, it is very likely to disturb or at least alter the status of the heart. There has been indeed some evidence against the validity of the time-varying elastance model with an assist device [18].

To face this challenge, in this paper, we propose a synergistic model which couples mechanical, electric, and chemical activity on microscale sarcomere and macroscale heart levels and investigate the effect of an axial rotary pump (e.g., Heart Mate II) on a failing heart. Our focus is to find an alternative method that is readily available within the constraints of the clinical environment. Lumped-parameter models are well suited for this purpose. We, thus, develop a comparable lumped-parameter model that predicts a P–V loop and LVAD–heart interaction by evolving left ventricular pressure and volume simultaneously at the minimum computational cost, instead of using the time-varying elastance concept.

Specifically, we propose the two types, which have the same mechanical or chemical and electric activity set up but different circulation models. depending on the coupling between the left ventricle and the systemic arterial circulation—the basic (extended) model without (with) coupling to the systemic arterial circulation. Our models consist of 9 or 12 ordinary differential equations, and thus require significantly less computational resources and time compared with more advanced models [19] governed by partial differential equations. In particular, [19] simulated left ventricular fluid–solid mechanics through the cardiac cycle under LVAD support. CircAdapt [20] is another example of advanced models incorporating electric and sarcomere dynamics, but a systematic study with LAVD seems lacking.

2. Materials and Methods

2.1. Mechanical/Chemical Model

On a microscale, we utilize the Bestel–Clement–Sorine (BCS) model of the dynamics of the contractile element [21–23] to evolve the active stress τ_c, stiffness k_c, strain ε_c, and its velocity $v_c = \frac{d\varepsilon_c}{dt}$. In the BCS model, the active force derives from the chemical activity (e.g., ATP) modeled by u (measured in s^{-1}). The governing equations for v_c, ε_c, τ_c, and k_c are then as follows:

$$\frac{dv_c}{dt} = -\chi v_c - \omega_0^2 \varepsilon_c - a\tau_c d_0(\varepsilon_c) + b\left(\sqrt{\frac{V}{V_0}} - 1\right), \tag{1}$$

$$\frac{d\varepsilon_c}{dt} = v_c, \tag{2}$$

$$\frac{d\tau_c}{dt} = k_c v_c - (\alpha_l |v_c| + |u|)\tau_c + \sigma_0 u \Theta(u), \tag{3}$$

$$\frac{dk_c}{dt} = -(\alpha_l |v_c| + |u|)k_c + k_0 u \Theta(u), \tag{4}$$

$$d_0(\varepsilon_c) = \exp\left(-\beta_0 (\varepsilon_c)^2\right). \tag{5}$$

Here, $\Theta(u)$ is a Heaviside function that takes the value of 1 for $u > 0$ or 0 otherwise. The evolution of v_c in Equation (1) involves a damping force χv_c, a harmonic force $\omega_0^2 \varepsilon_c$, an active force $a\tau_c d_0(\varepsilon_c)$, and a passive force $b(\sqrt{V/V_0} - 1)$, where χ, a, b, α_l are positive constants. Here, ω_0 is a microscale, high-oscillation frequency. Equation (1) is based on a simplified model of a cylindrical heart with a constant height [23], where the left ventricular volume V is related to the strain ε as a square root $\varepsilon \propto \sqrt{V}$. In Equations (3) and (4), the term involving $\alpha_l |v_c| + |u|$ represents the deactivation of contractile force, while the term involving $u\Theta(u)$ represents its activation due to a chemical input $u > 0$. Additionally, $d_0(\varepsilon_c)$ in Equations (1) and (5) represents the length–tension curve of the contractile element, which we model using a Gaussian function for simplicity. The form of Equations (1)–(4) is identical to the BCS model.

To further link microscale dynamics in Equations (1)–(5) to macroscale dynamics, we relate τ_c in Equations (1) and (3) to the left ventricular pressure P_V [23]:

$$P_V = \gamma \frac{V_0}{V} [d_0(\varepsilon_c)\tau_c + \sigma_P], \tag{6}$$

$$\sigma_P = \frac{k_2}{k_1} [\exp(k_1 \sqrt{V/V_0} - 1) - 1], \tag{7}$$

where σ_P represents the passive stress, which is assumed to be exponential in Equation (7) for simplicity; k_1 and k_2 are non-negative parameters for the passive tension. In Equation (6), γ is a constant parameter proportional to the ratio of left ventricular wall thickness to its radius, and its physiological meaning is provided in [21]. For our purpose of coupling microscale and macroscale dynamics, it suffices to treat this constant as a parameter proportional to the above ratio and tune it.

2.2. Electric Activity Model

We now link the chemical activity u in Equations (3) and (4) to the electric activity. To this end, we adapt the forced Van der Pol [2] and FitzHugh–Nagumo [24] models for our convenience (the precise form is not particularly important, given the nonlinearity of the equations), as follows:

$$\frac{dp}{dt} = 0.1(q - p + \mu_1 \tau_c), \tag{8}$$

$$\frac{dq}{dt} = 10q\left(1 - q^2\right) - 10(2\pi)^2 p + \mu_2 V \Theta(V - V_0) + 10\cos(2\pi t), \tag{9}$$

$$u = \alpha_u q, \tag{10}$$

where p and q are dimensionless slow and fast variables for the electric activity, respectively; $10\cos(2\pi t)$ in Equation (9) represents the force with 1 Hz frequency, which we fix to model a normal heart with heart rate 1 Hz as a control case. Equation (10) represents the chemical activity u proportional to electric activity (q) with a proportional constant $\alpha_u > 0$. Here, μ_1 and μ_2 in Equations (8) and (9) represent the mechano-electric feedback (MEF) [25–29]. The non-zero value of μ_1 or μ_2 introduces the coupling between (p, q) and τ_c or V. Specifically, μ_1 mimics the effect of mechanical stress due to shortening during a contraction on the action potential and is motivated by [25]; μ_2 models the effect of stretch (e.g., through a stretch-activated ion channel) [28]. Biologically, the values of μ_1 and μ_2 could be changed due to the over or under expression of an ion channel. The units of μ_1 and μ_2 are kpa^{-1} and $(s \cdot mL)^{-1}$, respectively. Since the role of MEF in a beating heart is implicit, we are uncertain about the absolute value or sign of μ_1 and μ_2 for a control case. However, we find that $\mu_1 = 0.0024$ kpa^{-1} gives a

reasonable relaxation time (about 0.4~0.5 s for 1Hz heart rate). We, thus, choose $\mu_1 = 0.0024$ kpa^{-1} and $\mu_2 = 0$ for a control case. In the remainder of the paper, we omit the units of μ_1 and μ_2 for simplicity.

2.3. Basic Circulation Model and Control Case

For the circulation model, at the simplest level, we ignore the dynamics of the systemic arterial circulation and propose the following basic model, which evolves the left ventricular volume V, aortic pressure m, and pump flow n through an axial rotary pump

$$\frac{dV}{dt} = \frac{1}{R_M}(P_R - P_V)\Theta(P_R - P_V) - \frac{1}{R_A}(P_V - m)\Theta(P_V - m) - \delta_p n, \tag{11}$$

$$\frac{dm}{dt} = -\frac{1}{C_S R_c}(m - m_0) + \frac{1}{C_A R_A}(P_V - m)\Theta(P_V - m) + \delta_p \frac{n}{C_A}, \tag{12}$$

$$\frac{dn}{dt} = \frac{\delta p}{L_*}\left[P_V - m - R_* n + \beta\omega^2\right]. \tag{13}$$

In Equation (12), m is not coupled to the aortic flow but instead has a parameter m_0, which models a constant arterial pressure. In Equation (11), P_R is the atrial pressure, and for our basic model, we take this as a constant value instead of treating it dynamically. Increasing P_R and m_0 has the effect of increasing preload and afterload, respectively. Equations (11) and (13) are exactly the same as those in [14,15]. Here, δ_p is a parameter to denote the presence of a pump, where $\delta_p = 1$ ($\delta_p = 0$) represents the presence (absence) of a pump. R_c, R_M, R_A, and R_* are resistances, C_S and C_A are compliances, and L_* is inertance. Equation (13) shows that the pump flow n through an axial pump is driven by $\beta\omega^2$, where β is the pump parameter and ω is the pump speed (not angular frequency), following the same notations as in [5,14,15]. Variables and parameters in Equations (1)–(12) are summarized in Tables 1 and 2, respectively, together with their physiological meaning and their values.

Table 1. Summary of variables and meanings.

Variable	Physiological Meaning (Unit)
v_c	Velocity of the contractile element (s^{-1})
ε_c	Strain of the contractile element
τ_c	Active tension of the contractile element (mmHg)
k_c	Stiffness of the contractile element (mmHg)
σ_P	Passive stress (mmHg)
u	Chemical activity (s^{-1})
p	Slow electric variable
q	Fast electric variable
P_V	Left ventricular pressure (mmHg)
V	Left ventricular volume (mL)
P_R	Atrial pressure (mmHg)
P_S	Arterial pressure (mmHg)
m	Aortic pressure (mmHg)
m_0	Arterial pressure parameter for the basic model (mmHg)
F_a	Aortic (total) flow (mL/s)
n	Pump flow (mL/s, mL/min)
δ_p	Pump parameter (1 for pump, 0 for no pump)

Note that the parameter values for the contractile components (σ_o, k_c, k_1, k_2) are based on [21–23], while those for resistance, compliance, inertance, pump, and are taken from [14,15]. The advantage of this basic model is that solutions are not too sensitive to initial conditions due to the nonlinearity of Equations (1)–(10) for mechanical and electric activity and the fixed value of P_R and m_0 in the circulation model in Equations (11) and (12), allowing us to find (almost) unique solutions after initial transients disappear.

Table 2. Typical model parameters. The pathological case is in square brackets.

Parameter	Value	Physiological Meaning
R_A	0.001 mmHg s/mL	Aortic valve resistance
R_M	0.005 mmHg s/mL	Mitral valve resistance
R_S	0.5 mmHg s/mL	Systemic vascular resistance
R_C	0.0398 mmHg s/mL	Characteristic resistance
R_*	$0.3061 - 3.5\,(P_V - 1\;mmHg)\,\Theta(1\;mmHg - P_V)$	Total pump resistance
C_R	4.4 ml/mmHg	Left atrial compliance
C_S	1.33 ml/mmHg	Systemic compliance
C_A	0.08 ml/mmHg	Aortic compliance
L_S	0.0005 mmHg·s^2/mL	Inertance of blood in aorta
L_*	0.0472 mmHg·s^2/mL	Total pump inertance
σ_0	240 kpa	Maximum sarcomere active tension
k_0	120 kpa	Maximum sarcomere active elastance
k_1	0.002 kpa	Model parameter for a passive tension
k_2	14 kpa [40 kpa]	Model parameter for a passive tension
$\chi,\ \alpha_l$	100 s^{-1}, 10 m^{-1}	Damping parameters in sarcomere
ω_0	100 s^{-1}	Sarcomere microscale oscillation frequency
$a,\ b$	100 m·s^{-2} kpa^{-1}, 6000 m·s^{-2}	Active and passive force parameters
β_0	20 mL^{-2}	Length-tension parameter
γ	0.6 [0.45]	P_V parameter
V_0	144/1.5 mL [144 mL]	Volume parameter
$\mu_1,\ \mu_2$	0.0024 kpa^{-1}, 0 (s·mL)$^{-1}$	MEF parameters

2.4. Extended Circulation Model and Control Case

We extend our basic model by incorporating the dynamics of the systemic arterial circulation, specifically by treating the arterial and atrial pressures dynamically. We, thus, include the following evolution of Equations (16) and (17) for atrial pressure P_R and arterial pressure P_S based on the Windkessel model in [14,15], while generalizing Equation (12) to Equations (14) and (15) by including the aortic flow F_a:

$$\frac{dm}{dt} = -\frac{1}{C_A}F_a + \frac{1}{C_A R_A}(P_V - m)\Theta(P_V - m) + \delta_p \frac{n}{C_A}, \tag{14}$$

$$\frac{dF_a}{dt} = \frac{m - P_S}{L_S} - \frac{R_C F_a}{L_S}, \tag{15}$$

$$\frac{dP_R}{dt} = \frac{-P_R + P_S}{C_R R_S} - \frac{1}{C_R R_M}(P_R - P_V)\Theta(P_R - P_V), \tag{16}$$

$$\frac{dP_S}{dt} = \frac{P_R - P_S}{C_S R_S} + \frac{F_a}{C_S}, \tag{17}$$

where R_S is the systemic vascular resistance. Thus, for our extended model, we solve Equations (14)–(17), (1)–(11) and (13) using parameter values in Table 2. Equations (14)–(17) are identical to those in [14,15], with $P_R = x_2$, $P_S = x_3$, $m = x_4$, $F_a = x_5$ ($V = x_1$, $n = x_6$), with the key difference that we calculate V and P_V through the coupling to the microscale dynamics instead of using a prescribed time-varying elastance formula. Figure 1 shows the electric circuits for the basic model in Figure 1a and for the extended model in Figure 1b, where the detailed explanation is provided in the figure caption.
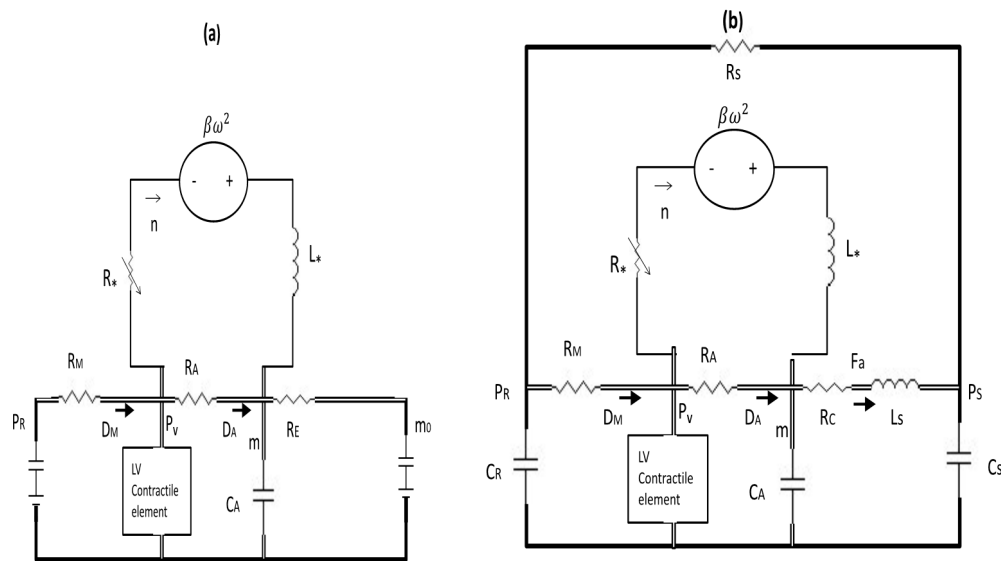
Figure 1. (**a**) The electric circuits for the basic model (**a**) and for the extended model (**b**). For the pump part, only total (effective) inductance L_* and resistance R_* are shown.

Here, D_M and D_A represent diodes; (a) $R_E = R_C \frac{C_S}{C_A} > R_C$ and constant values of P_R and $P_S = m_0$ are represented by batteries. To recover the basic model from the extended model, we let $R_C \to R_E$ and $P_S \to m_0$ in Equation (15) and obtain the steady solution $F_a = \frac{m - P_S}{R_E} = \frac{m - m_0}{R_C C_S} C_A$. Substituting this in $\frac{1}{C_A} F_a$ in Equation (14) then gives $\frac{m - m_0}{R_C C_S}$ in Equation (12).

3. Results and Discussions

3.1. Control Case in Basic Model

As an example of a control case, we choose $P_R = 9$ mmHg, $m_0 = 70$ mmHg, $b = 6000$, $\gamma = 0.6$, $k_2 = 14$ kpa, $\alpha_u = 5$, $V_0 = 144/1.5$ mL, $\mu_1 = 0.0024$, and $\mu_2 = 0$. The initial left ventricular volume is taken as $V(t = 0) = 0.5 \, V_0$. For this basic model, solutions do not sensitively depend on other initial values, and settle into (almost) unique solutions quickly (after a few seconds). Figure 2 shows the time evolution of V/V_0 and ε_c in Figure 2a, τ_c and k_c in Figure 2b, q, p in Figure 2c, and P_V and m in Figure 2d, where they all quickly move to a steady state from after only one or two transient oscillations. The initial transient is not shown in the P–V loop in Figure 2e. In Figure 2f, we show the elastance $E(t) = \frac{P_V}{V(t) - V_*}$ by using the volume at zero pressure $V_* \sim 7$ mL, which is determined from the end systolic pressure–volume relation (ESPVR) and shown by a solid red line in Figure 3a for steady-state P–V loops obtained for different m_0 values.

Figure 3a reveals that the larger the afterload m_0, the larger the end systolic volume (ESV) and the smaller the stroke volume (SV = EDV − ESV), where EDV is the end diastolic volume. In Figure 2f, the maximum and minimum values of $E(t)$ are about 2.1 and 0.07 mmHg/mL, respectively, similar to those that are used for the time-varying elastance model for a normal heart [14,15]. Furthermore, the overall shape and time duration between contraction and relaxation are also qualitatively similar to those from the time-varying elastance model. This is shown in Figure 3b by magnifying Figure 2f. For larger values of m_0, the ESPVR is observed to be concave to the volume axis, consistent with the experimental results [17,30].
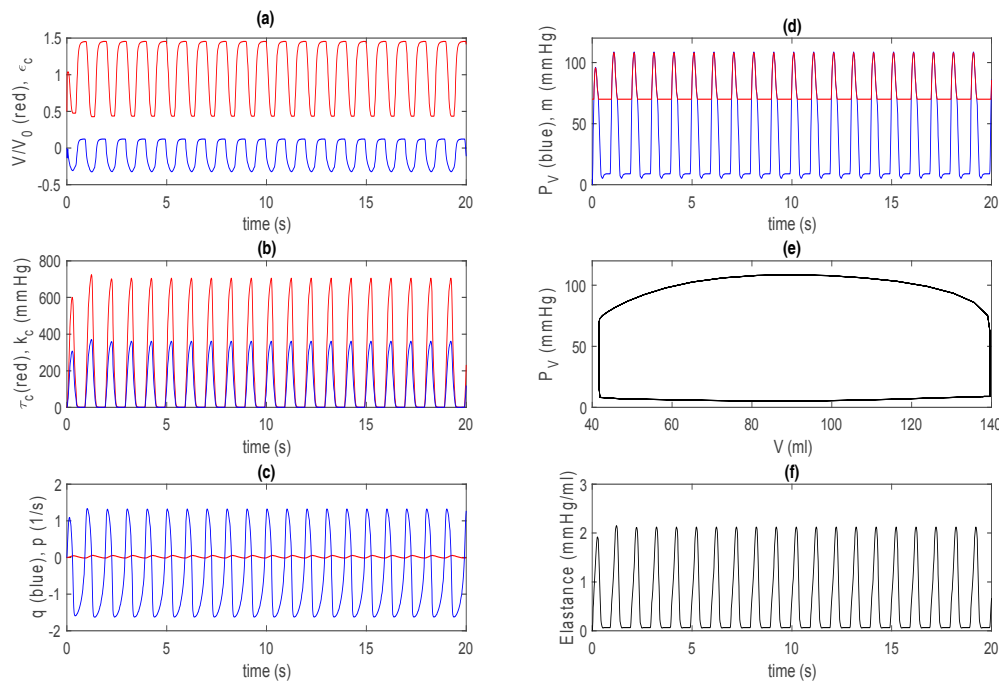
Figure 2. Control case for the basic model. (**a**) The V/V_0 (red) and ε_c (blue) against time; (**b**) τ_c (red) and k_c (blue) against time; (**c**) q (blue) and p (red) against time; (**d**) P_V (blue) and m (red) against time; (**e**) P_V against V; (**f**) elastance against time.
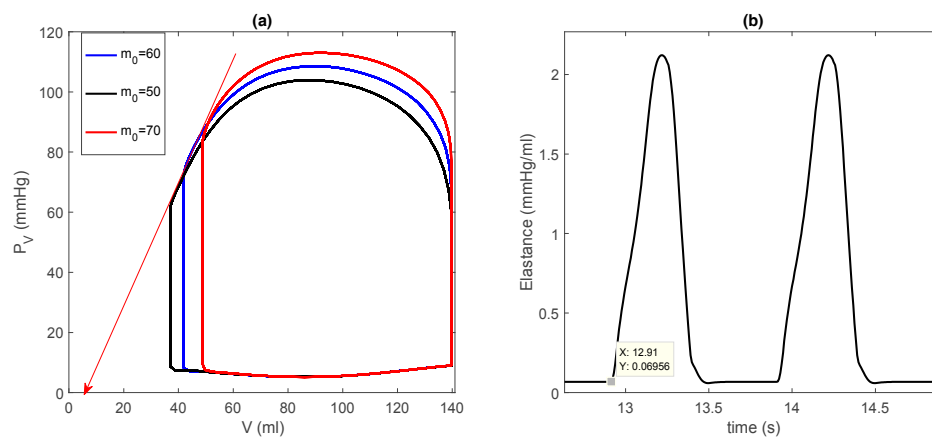

Figure 3. (**a**) Steady-state pressure–volume (P–V) loops for different afterloads: $m_0 = 50$, 60 and 70 mmHg; (**b**) $E(t)$ in Figure 2f for the basic model. Note that a data cursor image shows E_{min} on the y-axis.

3.2. Control Case in Extended Model

For the extended model, we use the same parameter values as in Figures 2 and 3 (e.g., $k_2 = 14$ kpa, $\gamma = 0.6$, $V_0 = 144/1.5$ mL, etc.) and in Table 2. Since the circulation models for P_R, m, P_S, and F_a are linear, solutions have a rather sensitive dependence on initial values in addition to parameter values. For Figure 4f, we use initial values $P_R(0) = 10$ mmHg, $P_S(0) = 70$ mmHg, $m(0) = 70$ mmHg, $F_a = 90$ mL/s, and $V(t = 0) = 0.9\,V_0$. In Figure 4f, $E(t)$ is calculated by determining the zero pressure volume $V_* \sim 7$ mL (see Figure 5). Notably, the overall behaviour in Figure 4 is quite similar to that in Figure 2. In particular, the solutions go to a steady state form after only one or two transient oscillations in Figure 4a–d,f; The initial transient is not shown in the P–V loop in Figure 4e.

　　　Figure 5 is equivalent to Figure 3 and shows different P–V loops in a steady state obtained for different initial conditions $V(0) = [0.4, 0.5, 0.6, 0.7, 0.8, 0.9]$ mL, as well as a detailed view of $E(t)$ by magnifying Figure 4f. Interestingly, in Figure 5a, as $V(0)$ increases, both EDV and ESV increase, similar to the effect of different preloads through interactions between preload and afterload, where an increase in SV leads to an increase in cardiac output, arterial pressure, and thus, afterload. For $V(0) > V_0$, we observe that ESPVR is concave to the volume axis, as in the basic model. Furthermore, Figure 5b is quite similar to Figure 3b, with similar maximum (around 2.1 mmHg/mL) and minimum (around 0.06 mmHg/mL) values. These results underscore that the basic model is a good approximation of the extended model for a control case.
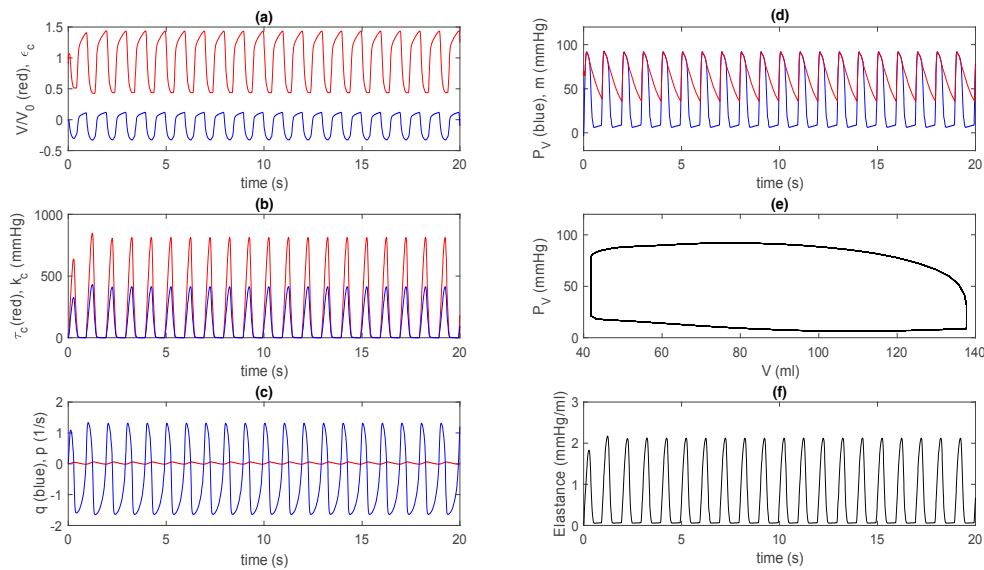
Figure 4. Control case for the extended model: (**a**) V/V_0 (red) and ε_c (blue) against time; (**b**) τ_c (red) and k_c (blue) against time; (**c**) q (blue) and p (red) against time; (**d**) P_V (blue) and m (red) against time; (**e**) P_V against V; (**f**) elastance against time.
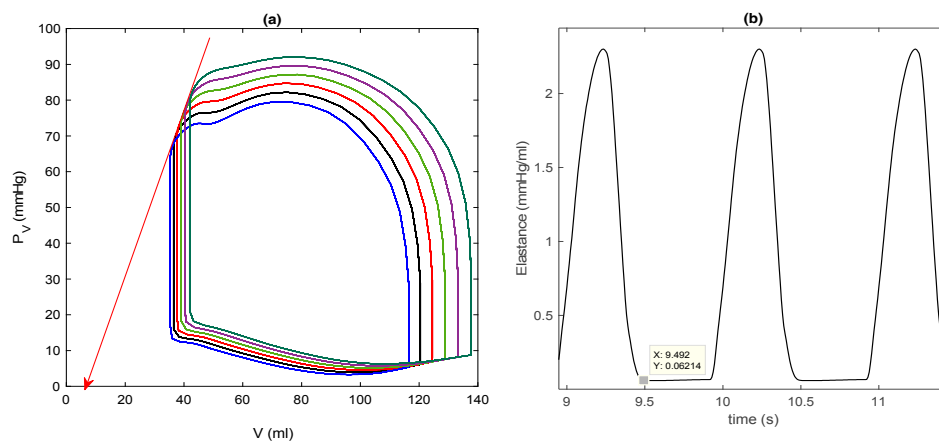
Figure 5. (**a**) Steady-state P–V loops for different afterloads: $V(0) = [0.4, 0.5, 0.6, 0.7, 0.8, 0.9]V_0$ increasing to the right; (**b**) $E(t)$ in Figure 4f for the extended model. Note that a data cursor image shows E_{min} on the y-axis.

3.3. Dilated Cardiomyopathy

　　　Dilated cardiomyopathy is one of the main causes of heart failure, where the heart becomes enlarged and cannot pump blood effectively. This can result from left ventricular remodeling, such as a gradual increase in left ventricular EDV and ESV, wall thinning, and other causes. To model this pathological change in heart geometry, we increase the parameter values of k_2 and V_0 to $k_2 = 40$ kpa,

$V_0 = 144$ mL while reducing γ to $\gamma = 0.45$ (these parameter values are in square brackets in Table 2) and fix all other parameter values.

3.3.1. Effect of a Pump on Dilated Cardiomyopathy in Basic Model

For all other parameters, we use the same values as those used in Figures 2 and 3. Figure 6 shows the time evolution of q (in blue) and p (in red) in the first column, a steady state P–V loop in the second column, and the evolution of pump flow n in the last column. The first row is for the case without a pump, where the zero pump flow simply means that there is no pump in this case. To see the effect of a pump, we choose $\delta_p = 1$ in Equations (11)–(13) and vary the values of rotary pump speed (frequency) ω in Equation (13) as $\omega = [0, 0.5, 1, 2] \times 8000$ rpm, presenting results in the second to fifth rows in Figure 6. As ω increases, the P–V loop initially shifts to a larger V before shifting to a smaller V. The pump flow is negative (associated with an increase in V) for $\omega = 0$ and then becomes positive (with the decrease in V) as ω increases. This means that the pump speed needs to exceed the minimum value to work effectively (a pump would shut down at the speed below this minimum value).

In clinical practice, 8000–10,000 rpm is the speed used for an axial rotary blood pump (HeartMate II) [10]. A speed < 8000 rpm is used when weaning off the LVAD and a certain protocol is followed, gradually decreasing the speed to 6000 rpm to allow ejection of the native heart and analyse its performance. In Figure 6, with the increase of ω, the left ventricular pressure P_V eventually decreases, while aortic pressure m increases. This implies that in a failing heart, a pump will help increase the arterial pressure. In the bottom row, we see the decoupling between P_V and m for $\omega = 2 \times 8000$ rpm. These results are similar to those from the time-varying elastance model [14,15].
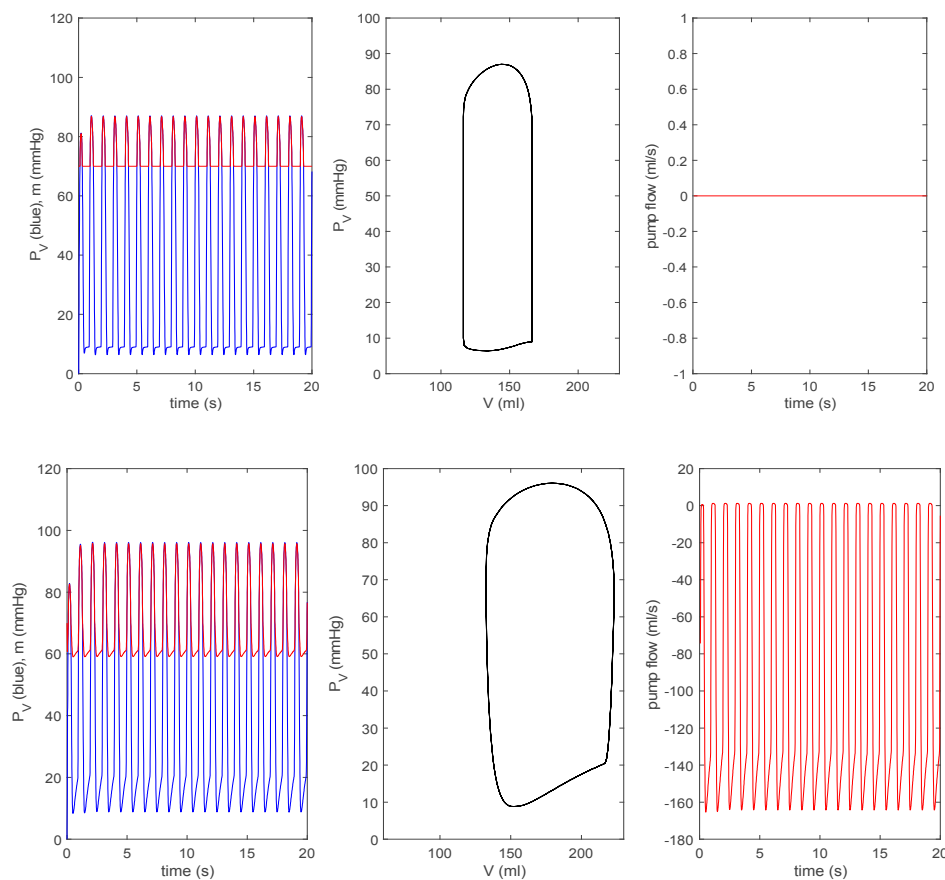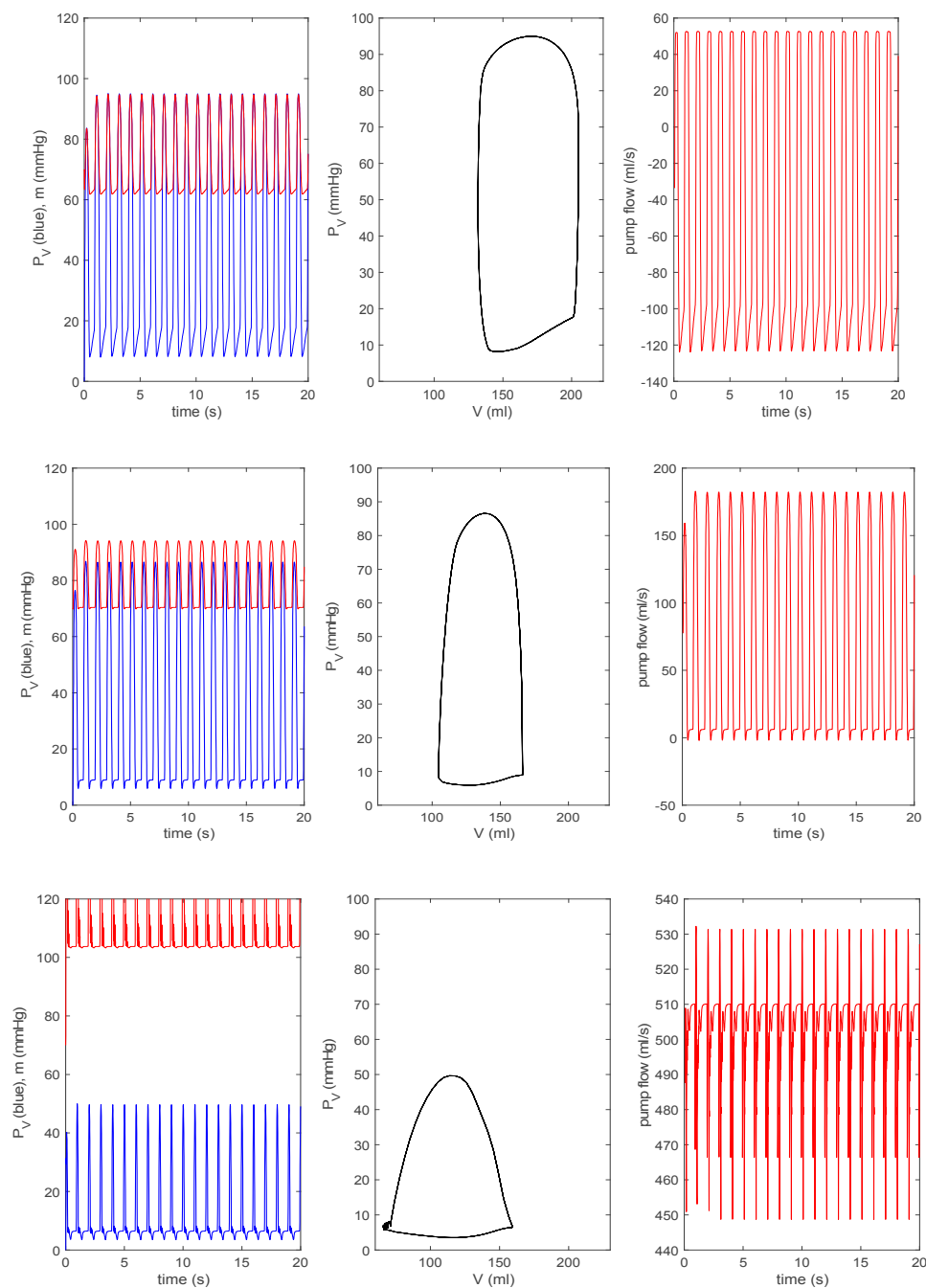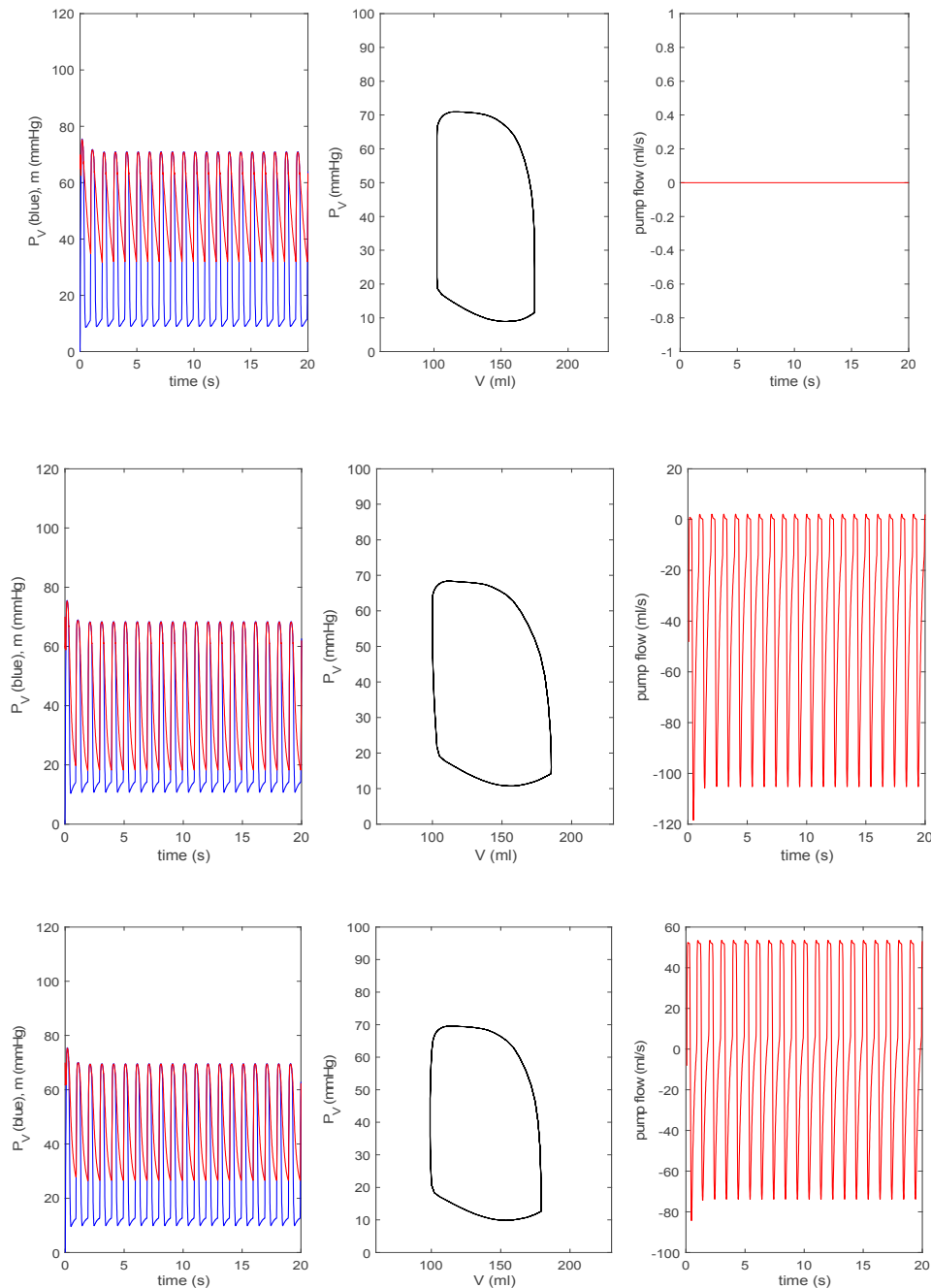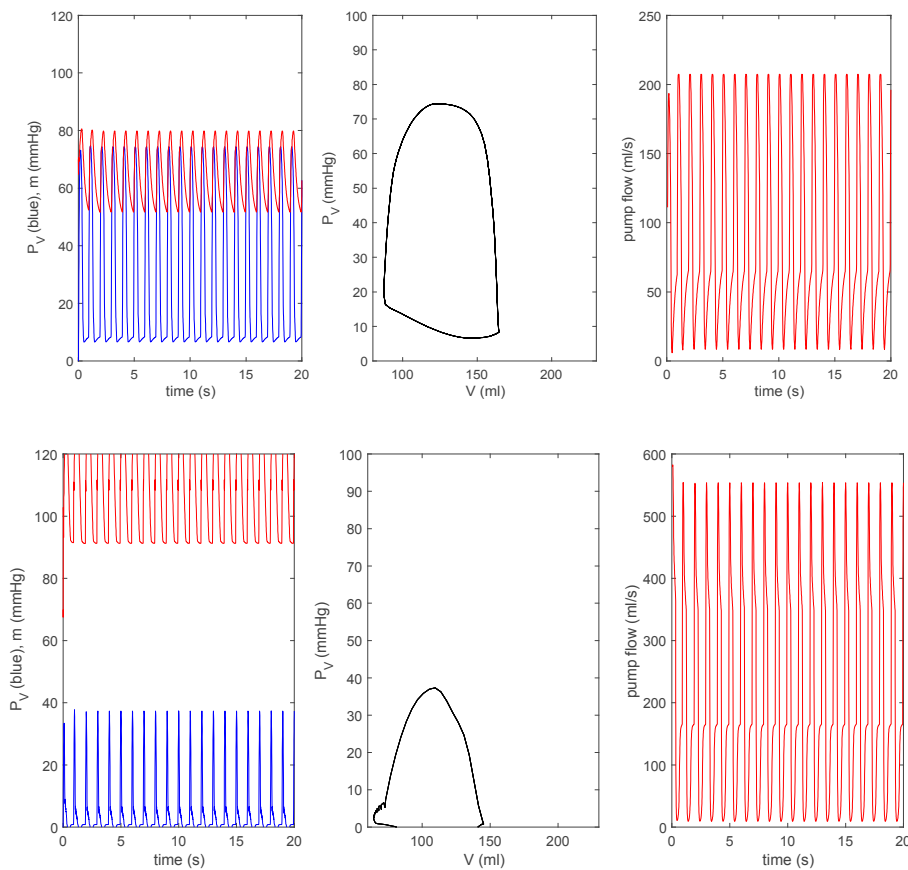

Figure 6. *Cont.*

Figure 6. From top to bottom: $\delta_p = 0$, $\omega = 0$, 0.5×8000, 8000, 2×8000 rpm, with $\delta_p = 1$ for the basic model. In each row, the left panel represents P_V (blue) and m (red) against time; the middle panel represents P_V against V; the right panel represents the pump flow n against time.

3.3.2. Effect of a Pump on Dilated Cardiomyopathy in Extended Model

For all other parameters, we use the same values as those used in Figures 4 and 5. Figure 7 is equivalent to Figure 6. The top row is the case without a pump ($\delta_p = 0$) for a pathological heart; the second to the bottom row in Figure 6 shows a pump ($\delta_p = 1$) with a pump speed $\omega = [0, 0.5, 1, 2] \times 8000$ rpm. As in Figure 6, as ω increases, a P–V loop initially shifts to a larger V before shifting to a smaller V; the pump flow becomes negative (related to the increase in V) before becoming positive (associated with the decrease in V). With the increase of ω, P_V (m) eventually decreases (increases). In the bottom row for $\omega = 2 \times 8000$ rpm, P_V and m decouple without any overlap between the two and P_V contains negative pressure. Overall, by comparing Figures 6 and 7, we observe the disparity in the behaviour of

n, in particular for $\omega = 2 \times 8000$ rpm. For a closer comparison with previous works [14,15], we make the pump speed a linearly increasing function of time as $\omega = 400\,t$ rpm and $\omega = 8000 + 200\,t$ rpm, and show the corresponding results together with the pump speed in the top and bottom panels of Figure 8, respectively. Overall, the behaviour of P_V, *m*, and *n* suddenly changes around $\omega \sim 12$ krpm, with the formation of a large envelope of oscillations. This nonmonotonic behaviour corresponds to the onset of the suction in [14,15]. For larger ω, P_V becomes negative.
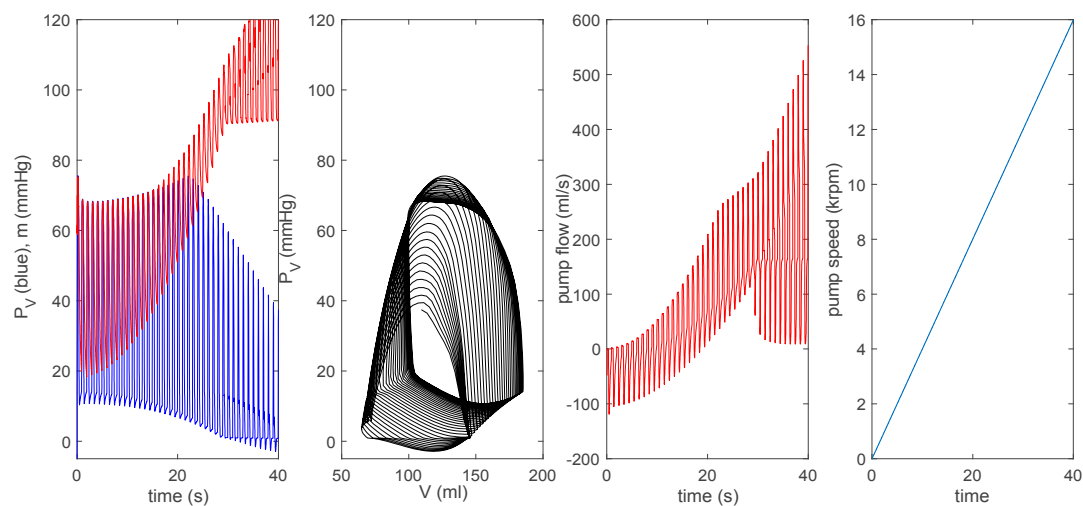

Figure 7. *Cont.*

Figure 7. From the top to the bottom: $\delta_p = 0$, $\omega = 0$, 0.5×8000, 8000, 2×8000 rpm, with $\delta_p = 1$ for the extended model. In each row, the left panel represents P_V (blue) and m (red) against time; the middle panel represents P_V against V; the right panel represents the pump flow n against time.

For a closer comparison with previous works [14,15], we make the pump speed a linearly increasing function of time as $\omega = 400\,t$ rpm and $\omega = 8000 + 200\,t$ rpm, and show the corresponding results together with the pump speed in the top and bottom panels of Figure 8, respectively. Overall, the behaviour of P_V, m, and n suddenly changes around $\omega \sim 12$ krpm, with the formation of a large envelope of oscillations. This nonmonotonic behaviour corresponds to the onset of the suction in [14,15]. For larger ω, P_V becomes negative.
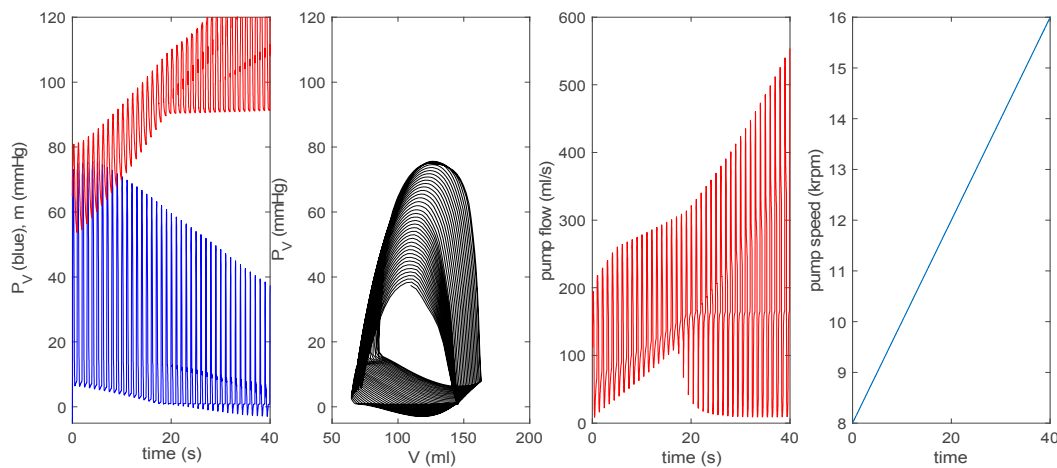

Figure 8. *Cont.*

Figure 8. The top shows $\omega = 400\,t$ rpm and the bottom shows $\omega = 8000 + 200\,t$ rpm for the extended model.

Further, to compare our results with in vivo animal data during rotary pump assistance (Figure 79.13 in [14], Figures 10 and 11 in [15]), we show results by using $\omega = 8000 + \frac{100t}{3}$ in Figure 9. In particular, the left bottom panel shows that the pump flow exhibits a large envelope of oscillations, while its mean value slowly increases over time; the onset of suction occurs at the pump speed $\omega \approx 12$ krpm. This is very similar to the behaviour of the pump flow from in vivo data shown in Figure 79.13 in [14].

Here, a substantial oscillation envelope is seen, with the mean value increasing with time before the onset of suction, which occurs at a similar pump speed of $\omega = 12.5$ krpm. In comparison, the evolution of the pump flow from the time-varying elastance model shown in Figure 79.12 in [14] behaves differently; there is a significant reduction in the oscillation envelope without much increase in its mean value before the onset of suction, and the onset of suction takes place at a much greater pump speed of $\omega \approx 15.5$ krpm.
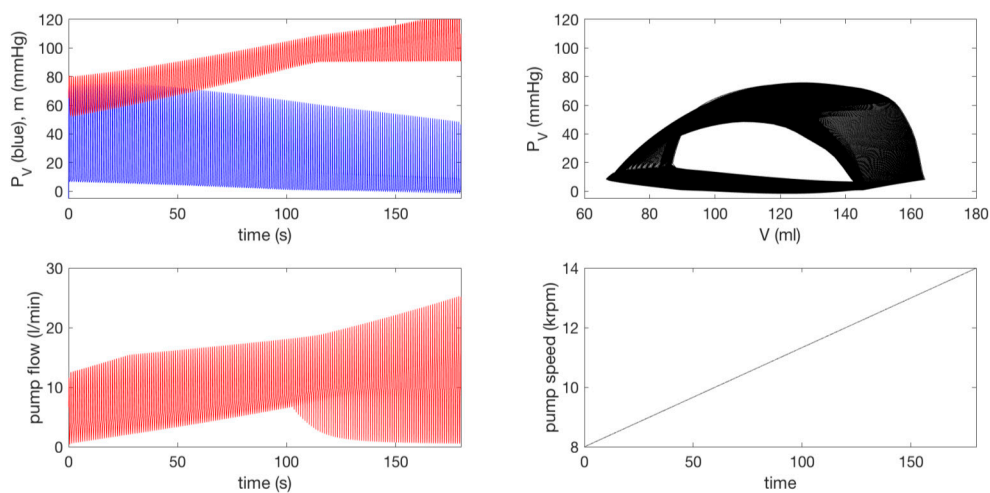

Figure 9. Here, $\omega = 8000 + 100t/3$ rpm for the extended model.

Therefore, our results are in much better agreement with in vivo data than the prediction from the time-varying elastance model in [14,15]. The agreement with in vivo data is also better in the extended model than the basic model, as aortic flow (its interaction with a pump) is not treated dynamically in the basic model (see Figure 10). These results highlight the importance of self-consistent treatment of the LVAD–heart interactions in simulating clinical scenarios, with a view to treatment optimization and outcome prediction.

Finally, we note that the direct comparison of our results with those from more advanced (distributed) models with the LVAD support [19] is difficult. if not impossible, because of the use of different variables or parameters and the lack of a systematic study on these advanced models (due to high computational cost).
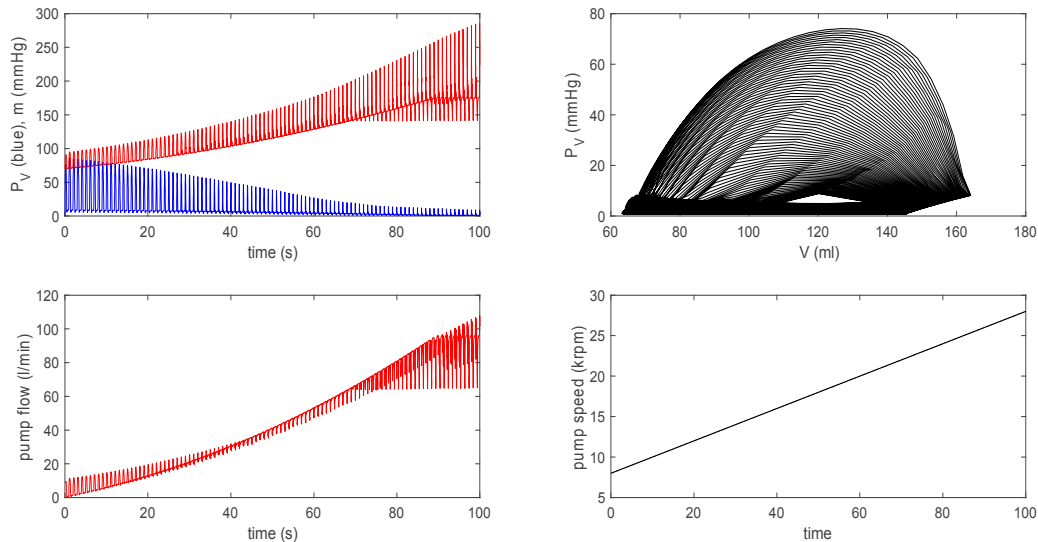

Figure 10. Here, $\omega = 8000 + 200\, t$ rpm for the basic model (compared with Figures 8 and 9 for the extended model).

3.4. Summary

The pressure–volume relation plays a key role in cardiovascular modeling, and the traditional approach heavily relies on the time-varying elastance concept [5,11–15], in which the pressure to volume ratio is prescribed as a (double) periodic function of time. In particular, lumped-parameter models combined with pressure–volume loop analysis and time-varying elastance are very effective in simulating clinical scenarios, with a view to treatment optimization and outcome prediction [6,11]. However, the time-varying elastance concept has limited validity, as it cannot address cardiac self-organization and its breakdown, especially for a mechanically supported left ventricle, where its application for the analysis of LVAD–heart interactions has been questioned. Therefore, our aim was to develop a method that is at least as good as lumped-parameter modeling, but which enables us to investigate cardiac self-organization and the interaction between the cardiac system and LVAD.

To this end, we developed a synergistic model that couples mechanical, electric, and chemical activity on microscale sarcomere and macroscale heart levels, and which predicted the pressure–volume relation of the left ventricle consistently. In a control case without LVAD, we showed that both basic and extended models reproduced the left ventricular pressure–volume relation, which is similar to what is obtained from the time-varying elastance model (e.g., comparing Figures 2–5 with Figure 79.8b in [14]).

We then considered a failing left ventricle by choosing parameter values to model dilated cardiomyopathy and investigated the interaction between a failing left ventricle and the circulation in the presence of a rotary pump by including the coupling between the aortic pressure and the pump flow in an axial rotary pump. For a sufficiently large pump speed, the stroke volume of the left ventricle increases, while its pressure and aortic pressure are decoupled with the increase (decrease) in the pressure of the aorta (left ventricle), similar to the finding from the time-varying elastance model. Furthermore, our extended model worked better than the time-varying elastance model in reproducing in vivo animal data with a rotary pump (see Figure 9), in particular in the overall shape (large envelope) of oscillations of the pump flow and the pump speed for the onset of suction, with a better agreement compared with the time-varying elastance model in [14,15].

4. Conclusions

We conclude that our synergistic model is a valid and better alternative to the time-varying elastance model considering that it addresses all the key aspects involved in terms of the overall P–V loop shape and the interaction between LVAD and circulation. In particular, it consistently incorporates the coupling between the mechanical and electric activity and can be used to explore MEF, which would otherwise have been impossible in real experiments or with the time-varying elastance model. The importance of self-consistent treatment of the LVAD–heart interactions was highlighted. Finally, we note that our model can also be extended to study the interaction between the left ventricle and atria [20], as well as the effect of LVAD on the right ventricle failure [31] at the simplest level, but yet is close to real life scenarios incorporating the interaction between the circulation, LVAD, and microscale dynamics. Future work will also explore the incorporation of central and peripheral extracorporeal membrane oxygenation (ECMO).

Limitation of our study: Given the simplicity of our lumped parameter model based on a set of ordinary differential equations, our model cannot inform us how our variables are distributed in space (e.g., waves), any consequences of their inhomogeneity, or the effect of boundaries. Furthermore, given the limited number of parameters, our model reproduces only a qualitatively similar shape of a P–V loop of an individual, but not its exact shape.

References

1. Haken, H. *Information and Self-Organization: A Macroscopic Approach to Complex Systems*; Springer Series in Synergetics; Springer: Berlin, Heidelberg, 2006.
2. Wright, T.; Twaddle, J.; Humphries, C.; Hayes, S.; Kim, E. Variability and degradation of self-organization in self-sustained oscillators. *Math. Biosci.* **2016**, *273*, 57–69. [CrossRef] [PubMed]
3. Sheikh, F.H.; Russell, S.D. HeartMate® II continuous-flow left ventricular assist system. *Expert Rev. Med. Devices* **2011**, *8*, 811–821. [CrossRef] [PubMed]
4. Tuzun, E.; Roberts, K.; Cohn, W.E.; Sargin, M.; Gemmato, C.J.; Radovancevic, B.; Frazier, O.H. In vivo evaluation of the HeartWare centrifugal ventricular assist device. *Tex. Heart Inst. J.* **2007**, *34*, 406–411.
5. Capoccia, M. Development and Characterization of the Arterial Windkessel and Its Role during Left Ventricular Assist Device Assistance. *Artif. Organs* **2015**, *39*, 138–153. [CrossRef]
6. Capoccia, M.; Marconi, S.; Singh, S.A.; Pisanelli, D.M.; De Lazzari, C. Simulation as a preoperative planning approach in advanced heart failure patients: A retrospective clinical analysis. *Biomed. Eng. Online* **2018**, *17*, 52. [CrossRef]
7. Ferrari, G.; Di Molfetta, A.; Zieliński, K.; Fresiello, L. Circulatory modelling as a clinical decision support and an educational tool. *Biomed. Data J.* **2015**, *1*, 45–50. [CrossRef]
8. Griffith, B.P.; Kormos, R.L.; Borovetz, H.S.; Litwak, K.; Antaki, J.F.; Poirier, V.L.; Butler, K.C. HeartMate II left ventricular assist system: From concept to first clinical use. *Ann. Thorac. Surg.* **2001**, *71*, 116–120. [CrossRef]
9. Giridharan, G.A.; Skliar, M.; Olsen, D.B.; Pantalos, G.M. Modeling and control of a brushless DC axial flow ventricular assist device. *Am. Soc. Artif. Intern. Organs (ASAIO) J.* **2001**, *48*, 272–289. [CrossRef]
10. Moazami, N.; Fukamachi, K.; Kobayashi, M.; Smedira, N.G.; Hoercher, K.J.; Massiello, A.; Lee, S.J.; Horvath, D.J.; Starling, R.C. Axial and centrifugal continuous-flow rotary pumps: A translation from pump mechanics to clinical practice. *J. Heart Lung Transplant.* **2013**, *32*, 1–11. [CrossRef]

11. Casas, B.; Lantz, J.; Viola, F.; Cedersund, G.; Bolger, A.F.; Carlhäll, C.J.; Karlsson, M.; Ebbers, T. Bridging the gap between measurements and modelling: A cardiovascular functional avatar. *Sci. Rep.* **2017**, *7*, 1–15. [CrossRef]

12. Suga, H.; Sagawa, K. Instantaneous pressure-volume relationships and their ratio in the excised, supported canine left ventricle. *Circ. Res.* **1974**, *35*, 117–126. [CrossRef] [PubMed]

13. Broomé, M.; Maksuti, E.; Bjällmark, A.; Frenckner, B.; Janerot-Sjöberg, B. Closed-loop real-time simulation model of hemodynamics and oxygen transport in the cardiovascular system. *Biomed. Eng. Online* **2013**, *12*, 69. [CrossRef] [PubMed]

14. Simaan, M.A. Rotary heart assist devices. In *Springer Handbook of Automation*; Nof, S.Y., Ed.; Springer: Berlin, German, 2009.

15. Simaan, M.A.; Ferreira, A.; Chen, S.; Antaki, J.F.; Galati, D.G. A dynamical state space representation and performance analysis of feedback-controlled rotary left ventricular assist device. *IEEE Trans. Control. Syst. Technol.* **2019**, *17*, 15–28. [CrossRef]

16. Shi, Y.; Korakianitis, T. Numerical Simulation of Cardiovascular Dynamics with Left Heart Failure and In-series Pulsatile Ventricular Assist Device. *Artif. Organs* **2006**, *30*, 929–948. [CrossRef] [PubMed]

17. Claessens, T.E.; Georgakopoulos, D.; Afanasyeva, M.; Vermeersch, S.J.; Millar, H.D.; Stergiopulos, N.; Westerhof, N.; Verdonck, P.R.; Segers, P. Nonlinear isochrones in murine left ventricular pressure-volume loops: How well does the time-varying elastance concept hold? *Am. J. Physiol. Heart Circ. Physiol.* **2006**, *290*, 1474–1483. [CrossRef]

18. Vandenberghe, S.; Segers, P.; Steendijk, P.; Meyns, B.; Dion, R.A.E.; Antaki, J.F.; Verdonck, P. Modelling Ventricular Function during Cardiac Assist: Does Time-Varying Elastance Work? *Am. Soc. Artif. Intern. Organs (ASAIO) J.* **2006**, *52*, 4–8. [CrossRef]

19. McCormick, M.; Nordsletten, D.A.; Kay, D.; Smith, N.P. Simulating left ventricular fluid-solid mechanics through the cardiac cycle under LVAD support. *J. Comput. Phys.* **2013**, *244*, 80–96. [CrossRef]

20. CircAdapt. Available online: http://www.circadapt.org/publications (accessed on 8 August 2019).

21. Bestel, J.; Clément, F.; Sorine, M. A biomechanical model of muscle contraction. In *International Conference on Medical Image Computing and Computer-Assisted Intervention*; Goos, G., Hartmanis, J., van Leeuwen, J., Eds.; Springer: Berlin, Germany, 2001; pp. 1159–1161.

22. Sainte-Marie, J.; Chapelle, D.; Cimrman, R.; Sorine, M. Modeling and estimation of the cardiac electromechanical activity. *Comput. Struct.* **2006**, *84*, 1743–1759. [CrossRef]

23. Bestel, J. Modèle diffréntiel de la contraction musculaire contrôlée: Application au système cardiovasculaire. Ph.D. Thesis, Université Paris 9, Paris, France, 2000.

24. FitzHugh, R. Impulses and physiological states in theoretical models of nerve membrane. *Biophys. J.* **1962**, *1*, 445–466. [CrossRef]

25. Knudsen, Z.; Holden, A.; Brindley, J. Qualitative modeling of mechano-electrical feedback in aventricular cell. *Bull. Math. Biol.* **1997**, *6*, 115–181.

26. Tse, G.; Wong, S.T.; Tse, V.; Lee, Y.T.; Lin, H.Y.; Yeo, J.M. Cardiac dynamics: Alternans and arhythmogenesis. *J. Arrhythm.* **2016**, *32*, 411–417. [CrossRef] [PubMed]

27. Franz, M.R. Mechano-electrical feedback in ventricular myocardium. *Cardiovasc. Res.* **1996**, *32*, 15–24. [CrossRef]

28. Lab, M.J.; Allen, D.G.; Orchard, C.H. The effects of shortening on myoplasmic calcium concentration and action potential in mammalian ventricular muscle. *Circ. Res.* **1984**, *55*, 825–829. [CrossRef]

29. Collet, A.; Bragard, J.; Dauby, P.C. Temperature, geometry, and bifurcations in the numerical modeling of the cardiac mechano-electric feedback. *Chaos Interdiscip. J. Nonlinear Sci.* **2017**, *27*, 093924. [CrossRef]

30. Burkhoff, D.; Sugiura, S.; Yue, D.T.; Sagawa, K. Contractility-dependent curvilinearity of endsystolic pressure-volume relations. *Am. J. Physiol. Heart Circ. Physiol.* **1987**, *252*, 1218–1227. [CrossRef]

31. Scardulla, F.; Agnese, V.; Romano, G.; Di Gesaro, G.; Sciacca, S.; Bellavia, D.; Clemenza, F.; Pilato, M.; Pasta, S. Modeling right ventricle failure after continuous flow left ventricular assist device: A biventricular finite-element and lumped-parameter analysis. *Cardiovasc. Eng. Technol.* **2018**, *9*, 427–437. [CrossRef]